



HAL
open science

Critical coupling in cavity-resonant integrated-grating filters (CRIGFs)

Elizabeth Hemsley, Olivier Gauthier-Lafaye, Antoine Monmayrant, Pascal Dubreuil, Stéphane Calvez, Anne-Laure Fehrembach, Evgeny Popov

► **To cite this version:**

Elizabeth Hemsley, Olivier Gauthier-Lafaye, Antoine Monmayrant, Pascal Dubreuil, Stéphane Calvez, et al.. Critical coupling in cavity-resonant integrated-grating filters (CRIGFs). *Optics Express*, 2023, 31 (17), pp.27274. 10.1364/oe.498125 . hal-04174761

HAL Id: hal-04174761

<https://laas.hal.science/hal-04174761>

Submitted on 1 Aug 2023

HAL is a multi-disciplinary open access archive for the deposit and dissemination of scientific research documents, whether they are published or not. The documents may come from teaching and research institutions in France or abroad, or from public or private research centers.

L'archive ouverte pluridisciplinaire **HAL**, est destinée au dépôt et à la diffusion de documents scientifiques de niveau recherche, publiés ou non, émanant des établissements d'enseignement et de recherche français ou étrangers, des laboratoires publics ou privés.



Critical coupling in cavity-resonant integrated-grating filters (CRIGFs)

ELIZABETH HEMSLEY,^{1,2} OLIVIER GAUTHIER-LAFAYE,¹ 
ANTOINE MONMAYRANT,^{1,*}  PASCAL DUBREUIL,¹
STÉPHANE CALVEZ,¹  ANNE-LAURE FEHREMBACH,²
AND EVGENY POPOV²

¹LAAS-CNRS, Université de Toulouse, CNRS, 7 Avenue du Colonel Roche, 31400 Toulouse, France

²Aix Marseille Univ, CNRS, Centrale Marseille, Institut Fresnel, F-13013 Marseille, France

*antoine.monmayrant@laas.fr

Abstract: We experimentally demonstrate critical coupling in miniature grating-coupled resonators known as cavity-resonant integrated-grating filters (CRIGFs). Using previously proposed asymmetric grating coupler designs for non-linear CRIGFs, and introducing a dedicated variant of a coupled-modes theory model to estimate physical properties out of the measured reflection and transmission characteristics of these resonators, we demonstrate fine control over the in-and out-coupling rate to the resonator while keeping constant both the internal losses and the resonant wavelength. Furthermore, the critical coupling condition is also observed to coincide with the maximum enhancement of the second harmonic generation signal.

© 2023 Optica Publishing Group under the terms of the [Optica Open Access Publishing Agreement](#)

1. Introduction

Cavity-resonant integrated-grating filters (CRIGFs) are planar waveguide Fabry-Pérot cavities embedding an intra-cavity surface grating coupler (GC). Their principle of operation is governed by the GC spectrally and spatially-mediated interaction of the incident free-space beam with the localized waveguide cavity modes. In that respect, CRIGFs are a particular implementation of BIC-class component [1–3], with the particularity that the bound mode volume is mesoscopic, larger than in PhC devices, and not fully delocalized as in classical planar BIC metasurfaces.

Exploiting this behaviour, CRIGFs have been used as wavelength-selective (directional)-waveguide couplers [4], and as (tunable)-filters [5–7] with a even-more specialized application as wavelength-control elements in extended-cavity diode lasers [8,9]. Should they include an (organic) gain layer, they have also been proven to enable laser (surface)-emission, case where they have become known as mixed-order distributed feedback lasers [10]. Similarly, when the constitutive layers exhibit high nonlinear susceptibilities such as when embedding a lithium niobate (LiNbO₃) layer, the resonant nature of the CRIGFs allows the demonstration of enhanced nonlinear frequency conversion and, in particular, of continuous-wave second harmonic generation (SHG) with sub-10mW input levels [11].

Recently, to improve the wavelength-selectivity or the stored energy in these cavities, we have theoretically and numerically shown that adjusting the GC coupling strength allows the CRIGF operation to be gradually changed from the overcoupled regime through the critically-coupled regime before reaching the undercoupled regime, and thereby optimize the device performance [12]. This allows us to tailor the optical response of the device in a somehow similar way to the absorption optimisation that was done in [13,14]. Our theoretical approach uses an asymmetric structure where the GC is simply shifted with respect to the centre of the Fabry-Pérot cavity established by the two lateral distributed Bragg reflectors (DBRs, see Fig. 1) [15,16]. Assuming that the localized mode is set by the cavity, the position of the GC tunes the alignment of its teeth with respect to the mode standing wave pattern and will thereby lead to a low (respectively

high) in/outcoupling extraction of the mode when the teeth match the mode intensity nodes (respectively anti-nodes), case referred as dark-mode (respectively bright-mode or conventional) CRIGFs [16].

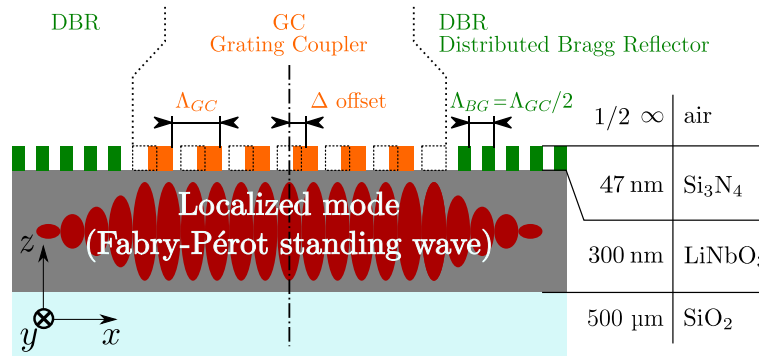


Fig. 1. Schematic view of the CRIGFs under study: two side distributed Bragg reflectors (DBR – green) form a planar Fabry-Pérot cavity supporting a resonant mode (standing wave – red), localized in the LiNbO₃ layer (gray); an asymmetric grating coupler (GC – orange) couples the resonant mode to an incident focused beam with coupling strength controlled by the asymmetry offset Δ .

In this manuscript, we experimentally study dark-mode CRIGFs operated in linear and nonlinear conditions and validate the influence of the GC coupling strength on the achievable device performance at both fundamental and SHG wavelengths. Moreover, since CRIGFs do not exhibit a clear signature in the (fundamental-wavelength) reflection/transmission characteristics associated with the critical coupling condition [12], contrary to waveguide ring resonators where the resonant transmission is minimal, we hereafter combine an analysis of the fundamental-wavelength and of the second harmonic signal responses to detect the critical coupling condition. To do so, we propose and validate a simplified model based on the coupled-mode theory suited for the extraction of physically-meaningful parameters from the recorded reflection and transmission spectra.

2. Sample design and fabrication

The device under study are asymmetric CRIGFs as proposed in [15] and further theoretically studied in [16]. Such structures are composed of a planar waveguide on which a cavity is created using two side distributed Bragg reflectors (DBRs, green on Fig. 1) creating a localized mode that is coupled to free space through a grating coupler (GC – orange). In the devices under study, the planar waveguide is made of a 47-nm-high Si₃N₄ layer deposited by plasma enhanced chemical vapour deposition (PECVD) on top of a x-cut lithium niobate on insulator (LNOI) substrate made of a 300-nm-thick LiNbO₃ layer on a 500-μm-thick fused silica substrate.

The GC and DBRs are defined in the Si₃N₄ layer during a single coupled plasma reactive ion etching (CCP-RIE) step with CHF₃-O₂ chemistry, using the lithium niobate layer as an etch stop layer. The GC is $N_{GC} = 21$ period-long and both DBRs are $N_{DBR} = 400$ -period long, for optimal reflectivity. Both GC and DBRs have a filling factor close to 50%. For the conventional design, the GC is centred in the Fabry-Pérot, with a periodicity $\Lambda_{GC} = \lambda_0/n_{\text{eff}}(\lambda_0)$ and the DBRs have a periodicity $\Lambda_{DBR} = \Lambda_{GC}/2 = \lambda_0/(2n_{\text{eff}}(\lambda_0))$ where $\lambda_0 = 1550$ nm is the wavelength of the resonant mode and $n_{\text{eff}}(\lambda_0) \approx 1.75$ the effective index inside the LiNbO₃ waveguide, resulting in $\Lambda_{GC} = 884$ nm and $\Lambda_{DBR} = 442$ nm. In the transverse direction (i.e. along the y-axis in Fig. 1) to the Fabry-Pérot cavity, the CRIGFs are 20-μm wide.

The key idea of the asymmetric design as described in [16] is that the coupling strength of the GC is determined by its spatial overlap with the localized standing wave. This allows to change the coupling strength of the GC by simply shifting its position in between the two DBRs by an asymmetry offset Δ . As the DBRs define the Fabry-Pérot cavity and set the position of the extrema of the localized mode, Δ changes the effective overlap between the mode and the GC, altering neither the GC geometry nor its feature size. Indeed, when the GC is in phase with the localized mode extrema ($\Delta = 0$), the coupling is maximal, while when the GC is shifted sideways by $\Delta = \Delta_{\pi/2} = \Lambda_{GC}/4 = 221$ nm, the GC and the localized mode are in quadrature and the coupling strength is null. Accordingly, the coupling strength evolves as $\cos^2(\theta)$ with $\theta = 2\pi\Delta/\Lambda_{GC}$ and this approach allows to finely tune the coupling strength over a wide range without any technological difficulties.

We thus fabricated, on a single sample, 42 CRIGFs with offsets Δ ranging from 0 to 410 nm by step of 10 nm, as shown in Fig. 2.

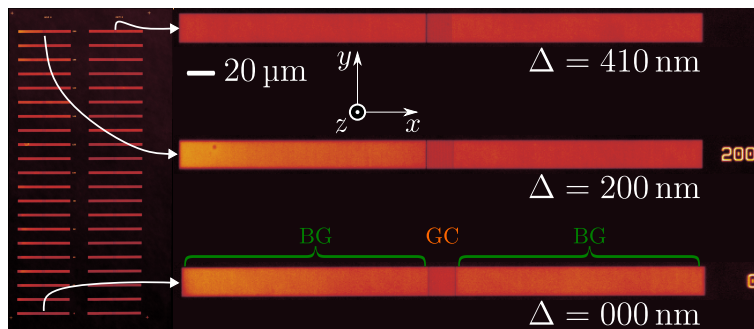


Fig. 2. Confocal microscope image of the 42 CRIGFs with varying offset Δ and zoomed images for the CRIGFs with $\Delta = 0$ nm, $\Delta = 200$ nm and $\Delta = 410$ nm.

3. Experimental setup and typical spectra

As shown on Fig. 3, the fabricated samples are characterized using a CW tunable telecom laser (Santec TSL-550) outputting up to $P = 10$ mW around $\lambda = 1550$ nm.

The incident laser beam is focused down to a waist of $w = 9$ μm with a 19-mm focal length lens and aligned on the GC of the CRIGF under study, with TE polarization (electric-field aligned with the y direction in Fig. 2). The reflected and transmitted spectra at the pump wavelength are recorded using two InGaAs photodiodes (Thorlabs PDA20CS-EC) while the generated second harmonic spectrum is measured using an avalanche photodiode (Thorlabs APD 440A). To increase the signal to noise ratio of the experiment, the laser intensity is modulated at ≈ 900 Hz using a chopper and all signals are recorded using lock-in detectors (Signal Recovery 7225). Reflection and transmission spectra are recorded for laser intensity of $P = 5$ mW and several second harmonic spectra (SHG) are recorded for laser intensities increasing from 1 to 10 mW. Typical spectra for SHG and linear reflection and transmission are presented in Fig. 4, for three different asymmetry offsets : $\Delta = 0$ nm (left column) and $\Delta = 130$ nm (centre column) and $\Delta = 220$ nm (right column).

On the linear spectra, the resonant coupling to the local mode of the CRIGF results in a single sharp peak in the reflection curves and a single sharp dip in the transmission curves. This is typical of an (asymmetric) Fano resonance where the light is coupled to the localized mode and its out-coupled part interferes (both in reflection and transmission) with the non-resonant contributions through the multilayer stack (oscillating reflection of about 10% in Figs. 4 (d), (e) and (f)). For the SHG signal, the resonant coupling to the local mode induces a strong

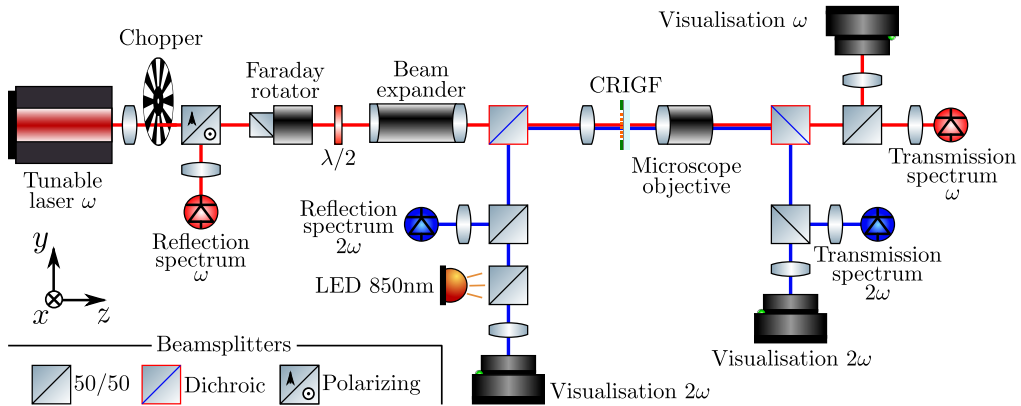


Fig. 3. Experimental setup.

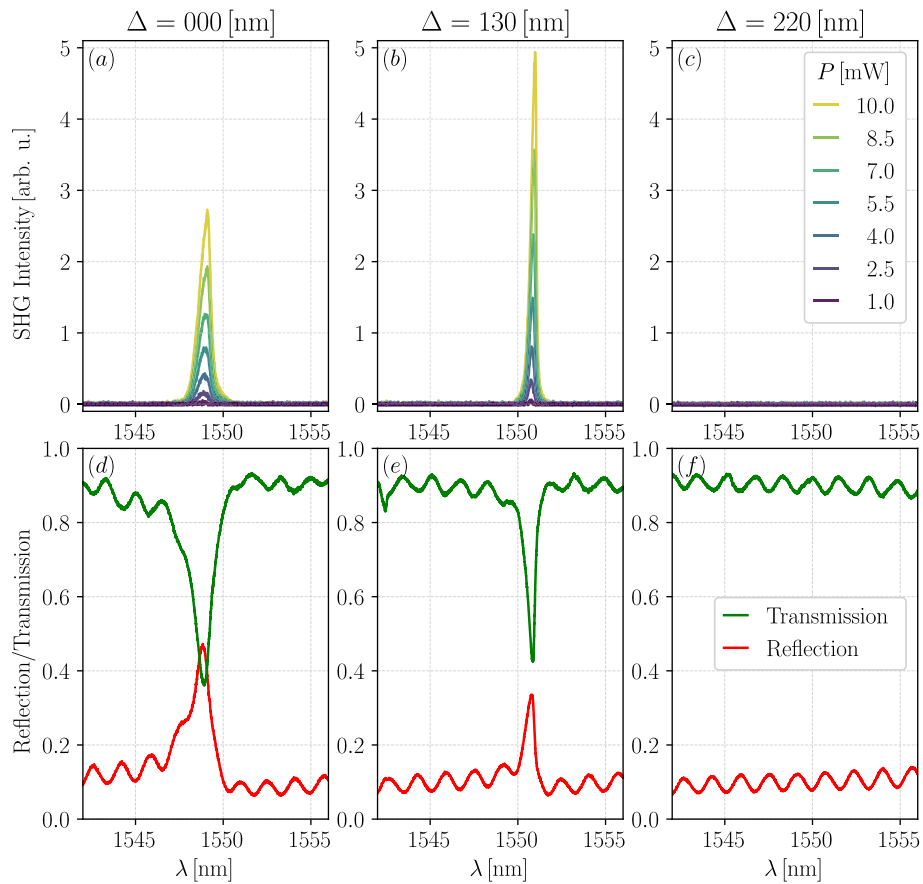


Fig. 4. (a), (b), (c) typical experimental SHG spectra for varying pumping power; (d), (e), (f) spectral reflection (red) and transmission (green). Results are presented for three offset values : $\Delta = 0$ nm (a) and (d), $\Delta = 130$ nm (b) and (e), and $\Delta = 220$ nm (c) and (f).

enhancement of the interaction with the lithium niobate layer resulting in a Lorentzian peak on a virtually dark background (as the non-linear conversion is negligible out of the resonance [11]). As expected, for $\Delta = 220$ [nm] $\approx \Delta_{\pi/2}$, the GC is in quadrature with the localized mode and its coupling strength is null. We thus do not observe any SHG (Fig. 4 (c)) and the transmission and reflection spectra correspond to those of the multilayer stack (Fig. 4 (f)). For intermediate Δ (for example $\Delta = 130$ nm), the SHG efficiency can be increased whilst the linear response decreases. The overall evolution of these spectra closely follow what was predicted in [16]. For increasing values of Δ in $[0, \Delta_{\pi/2}]$, the linear reflection spectra exhibit a peak with monotonous decrease of both its height and width, the peak completely disappearing for $\Delta \approx \Delta_{\pi/2}$ (Fig. 4 (f)). As for the SHG spectra (that are directly related to the square of the intensity of the excited mode in the cavity), they reach a maximum somewhere between $\Delta = 0$ and $\Delta = \Delta_{\pi/2}$ (Fig. 4 (b)).

4. Non-linear Fano coupling model

In order to determine the intrinsic losses of the various CRIGFs, together with the coupling strength offered by the asymmetric GCs, we used the hereafter-described model to fit the linear and non-linear responses from the CRIGFs under study.

The model is based on the temporal coupled-mode theory for Fano resonances in optical resonators introduced by Fan [17] and more specifically on the variant for lossy two-port systems proposed by Yoon [18]. We amend the latter model by separating the incoming free space beam into two modal components : one that interacts with the localized resonator and gives rise to a Fano resonance (i.e. it interacts with both the local resonator and the non-resonant stack), and the other one, orthogonal to the first component, which effectively by-passes the resonator, and only interacts with the non-resonant stack. We consider these two modal components as orthogonal, and will thus sum their contributions in intensity. This decomposition follows the approach used by Ding in [19] to model the coupling interaction between a singlemode waveguide and a multimode (ring) resonator.

We describe the spectra as functions of the reduced frequency usually used to describe Fano resonances, δ , whose expression is:

$$\delta = 2Q(\lambda_0 - \lambda)/\lambda_0 = 2Q(\omega - \omega_0)/\omega_0 \quad (1)$$

where λ_0 the central wavelength of the resonance, ω_0 the central frequency and Q is the quality factor as defined in [20].

The transmission, $T(\delta)$, and the reflection, $R(\delta)$ spectra, are then expressed as :

$$T(\delta) = \gamma T_i(\delta) + (1 - \gamma) T_d(\delta) \quad (2)$$

$$R(\delta) = \gamma R_i(\delta) + (1 - \gamma) R_d(\delta) \quad (3)$$

where $T_i(\delta)$ and $R_i(\delta)$ are respectively the spectral transmission and reflection for the interacting component of the beam expressed as in [18], and $T_d(\delta)$ and $R_d(\delta) = 1 - T_d(\delta)$ are the spectral transmission and reflection of the non interacting part of the beam (ie, in the absence of coupling to the local resonator, thus equal to the non resonant transmission and reflection) and $\gamma \in [0, 1]$ is the fraction of the incident beam that interacts with the resonator. In this model, γ describes the impact of partial modal overlap between the incident beam, the GC and the localized mode inside the resonator. This modal overlap is a central issue in the design and use of CRIGFs [21–23]. It can take into account some spatial overlap, but also imperfections of the incident beam if its phase profile or its polarization are not perfectly matching those required to optimally excite the local resonator.

Expanding the expressions of T_i and R_i from [18] in Eq. (2) and (3), one gets the following expressions for the transmission $T(\delta)$, reflection $R(\delta)$ and absorption $A(\delta)$:

$$T(\delta) = \underbrace{T_d(\delta)}_{\text{non resonant}} + \gamma \left[-\frac{4\eta_a\eta_r}{1+\delta^2}\alpha(1-\alpha) \right] + \underbrace{T_d(\delta)\eta_r \left(\frac{(q+\delta)^2}{1+\delta^2} - 1 \right)}_{\text{Fano}} \quad (4)$$

$$R(\delta) = 1 - T_d(\delta) + \gamma \left[-\frac{4\eta_a\eta_r}{1+\delta^2}\alpha^2 \right] + \underbrace{T_d(\delta)\eta_r \left(1 - \frac{(q+\delta)^2}{1+\delta^2} \right)}_{\text{Fano}} \quad (5)$$

$$A(\delta) = \underbrace{\left[\frac{4\eta_a\eta_r}{1+\delta^2}\alpha \right]}_{\text{Lorentzian}} \quad (6)$$

with parameters that follows closely those of reference [18]: η_a and $\eta_r = 1 - \eta_a$ are respectively the probability for the localized mode to be absorbed inside the sample or radiated. α (respectively $1 - \alpha$) is the fraction of radiation towards the reflection (respectively transmission) direction. q is the Fano shape factor which, upon trigonometric function simplification of the formula given in [18], can be expressed as:

$$q = p \sqrt{\frac{4\alpha(1-\alpha)}{T_d(\delta=0)} - 1} \quad (7)$$

where $p = \pm 1$ is the parity factor that governs the asymmetry of the Fano resonance (ie whether the zero is at shorter or longer wavelength than the maximum). This parity factor is determined by the phase of the reflection from the non resonant multistack. Here, $p = -1$.

The expressions of $T(\delta)$ in (4) and $R(\delta)$ in (5) contain each three terms: the first one corresponds to the non-resonant term coming from the contribution of the multistack alone, the second one to the Lorentzian contribution from the local resonator alone and the last one to the Fano term resulting from an interplay between the multistack and the resonator contributions. The resonant absorption $A(\delta) = 1 - R(\delta) - T(\delta)$ only contains a single term related to the resonator alone. These expressions of the reflection, transmission and absorption are the same as those proposed in ref [18], but for the scaling-down factor γ and the use of a more accurate spectrally-varying $T_d(\delta)$ function.

Fitting the linear response of our devices thus requires to evaluate 5 parameters: λ_0 , Q , η_r , α and γ . However, the non-linear response of the CRIGFs is directly linked to the field exaltation in the CRIGF by the Fano resonance [11]. As a result, it can provide meaningful initialization values for λ_0 and Q . Specifically, the SHG spectrum $S(P, \delta)$ is fitted using a Lorentzian function raised to the power of 2:

$$S(P, \delta) = P^2 \times \left(\frac{S_0}{(\delta^2 + 1)^2} \right) \quad (8)$$

where P is the pumping power and S_0 the SHG intensity for $P = 1$ mW and $\delta = 0$. With this model, the SHG field amplitude, proportional to the excited mode intensity is fitted by a Lorentzian.

Fitting the SHG spectra, we can determine Q and λ_0 for each asymmetric CRIGF, as well as S_0 which is proportional to the non-linear conversion efficiency of the device. A typical fit result is presented in Fig. 5, where the SHG spectra recorded for various pumping powers are all fitted simultaneously.

The fitted model from Eq. (8) reproduces accurately the wavelength and power dependence of the SHG emission, with narrow confidence intervals [24]. One subtle feature that is not taken into account in our simple model is the small redshift with increasing pump power. We attribute this drift to a residual optical absorption that thermally tunes the CRIGF [6] when the optical pump power is increased.

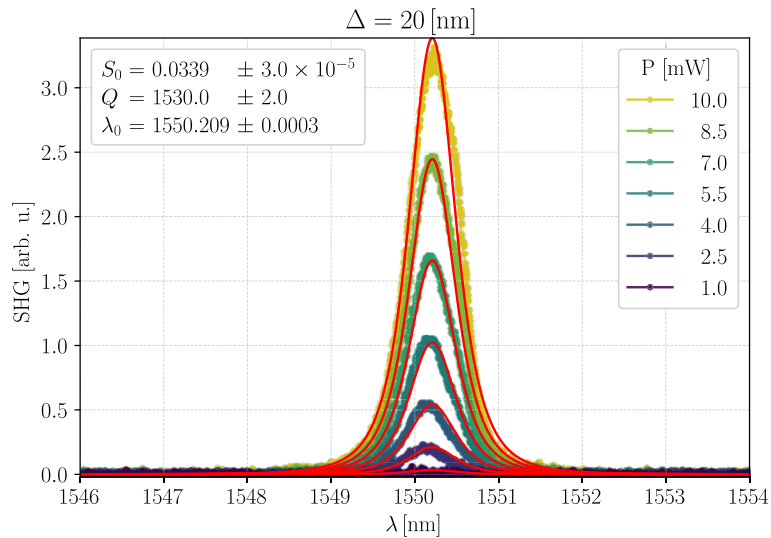


Fig. 5. Typical fit (red curve) of the experimental SHG spectra for varying pumping power (blue to yellow). The inset reports the fitted parameters with their confidence interval at 95 %.

The quality factor, Q , and wavelength of the resonance, λ_0 , are then used as initial guesses to fit the linear transmission and reflection spectra of the same CRIGF using Eqs. (4) and (5).

A typical result of this fitting procedure, here applied on the spectra measured for $\Delta = 20$ [nm], is shown in Fig. 6 for the reflection (left), transmission (centre) and absorption spectra (right). Experimental data (dots) are plotted with the results from our model (solid line) together with the model from [18]. The best-fit parameters obtained with our model and their associated 95 % confidence interval are listed in the inset.

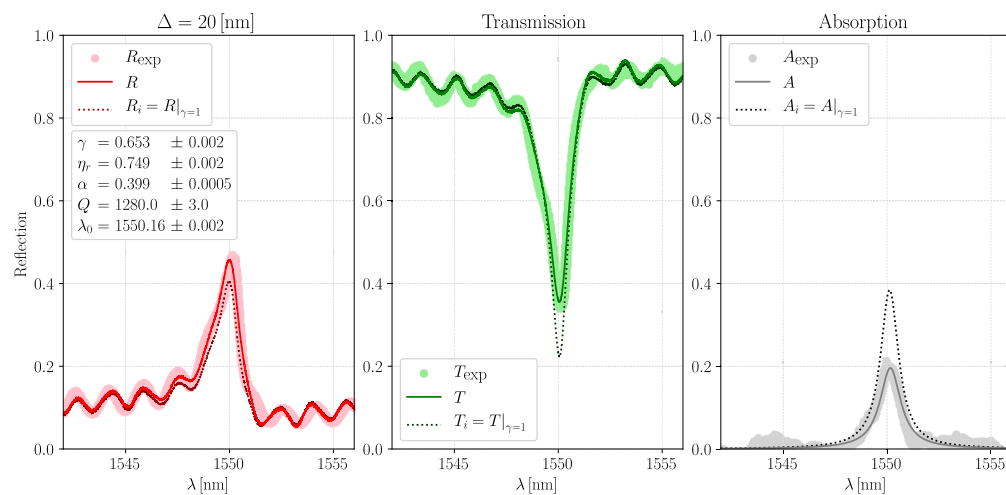


Fig. 6. Typical fit results for reflection (left), transmission (middle) and absorption (right), using our model (solid lines) and the model from ref [18] (dashed line) which correspond to our model with $\gamma = 1$. The inset reports the fitted parameters for our model, with their confidence interval at 95 %. The experimental spectra are denoted by points in light color and the subset $_{\text{exp}}$ in the legends.

First, we see that fitting with $\gamma = 1$, i.e. using the standard Fano modelling, does not allow for a proper estimation of $R(\delta)$ and $T(\delta)$. We found out that this model tends to systematically overestimate the losses in CRIGF structures (see Fig. 6 (left)), which, in turn, leads to an overestimate of the intrinsic losses η_a . Contrarily, with the above-proposed model, there is a better match to the experimental data, with good confidence intervals for the fitting parameters.

Moreover, comparing the fit results from Fig. 5 and Fig. 6, we can also see that the SHG spectrum analysis and the linear spectrum analysis lead to a good agreement for the resonant wavelength λ_0 , whilst the Q factors only differ slightly.

5. Experimental observations

This two-step fitting procedure was applied systematically for each of the fabricated CRIGFs. The fitted parameters from the SHG signal are presented in Fig. 7 as a function of the asymmetry offset Δ of each CRIGF.

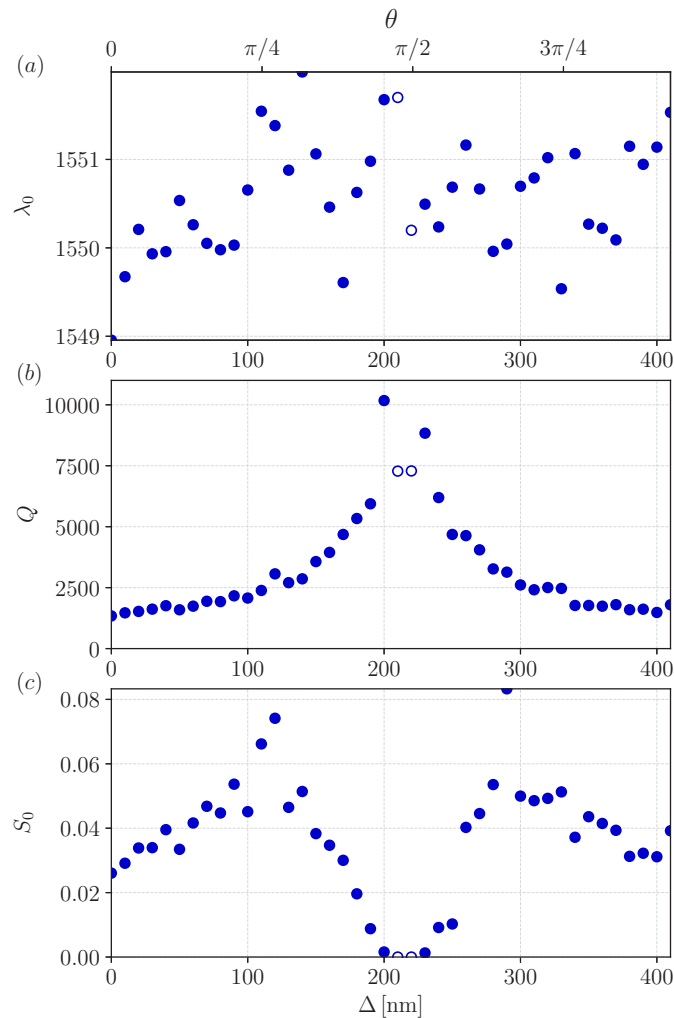


Fig. 7. Fitted SHG parameters (see Eq. (8)) as a function of the asymmetry offset Δ (blue dots). Open dots corresponds to offsets for which the SHG signal is null, and fit results unreliable.

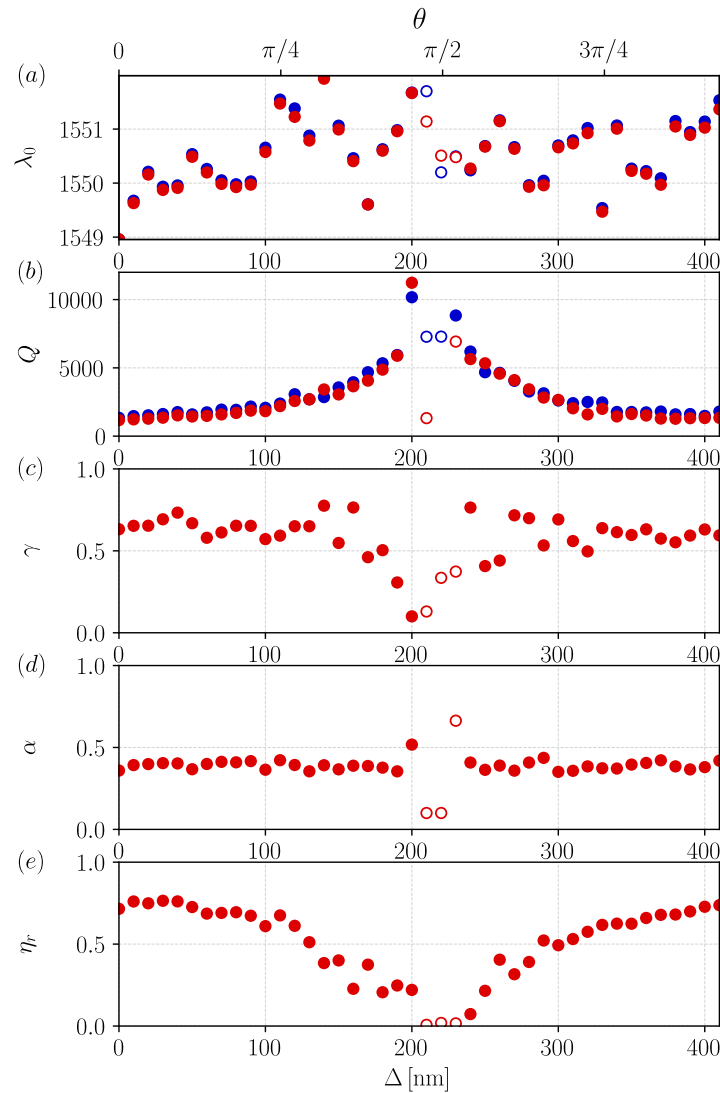


Fig. 8. Fitted parameters for R and T spectra (see Eqs. (4) and (5)) as a function of the asymmetry offset Δ (red). Open dots correspond to offsets for which the fitted parameters are unreliable. For λ_0 and Q , blue dots correspond to fitted parameters from the SHG signal.

As seen, the wavelength λ_0 exhibits small random variations (worst relative variation being around 0.1%). This provides a good indication of the homogeneity of the sample, but also shows that the GC only induces a small perturbation on the localized mode, thereby validating a property of this approach mentioned in [16].

The most interesting variations are observed for the quality factor, Q , and the conversion efficiency, S_0 , that are both symmetric with respect to the offset $\Delta = \Delta_{\pi/2} = 221$ nm. As Δ approaches $\Delta_{\pi/2}$ where the coupling losses through the GC are minimal, Q steadily increases, towards values larger than 5000, with even some extreme values about $Q \simeq 10000$ (note that for $\Delta = 210$ and 220 nm, no SHG can be observed). Moving away from $\Delta \simeq \Delta_{\pi/2}$, the coupling losses increase and Q decreases symmetrically.

The conversion efficiency S_0 exhibits two maxima, one on each side of $\Delta = \Delta_{\pi/2}$. We attribute these maxima to a balance between the intrinsic losses of the localized pump mode (that are independent of the GC coupling strength) and the amount of incoming/outgoing intensity actually coupled in the resonator (which increases with GC coupling strength). As will be shown below, each maxima corresponds to critical coupling in the (non-linear) CRIGF, where this balance is achieved.

The Fig. 8 shows the fitted parameters for the linear response (reflection and transmission) for each CRIGF (red dots), as a function of the asymmetry offset Δ . Open dots correspond to fitted parameters that are deemed unreliable because they exhibit confidence intervals that are significantly larger than the extracted values.

Like for the SHG analysis, the fitted parameters are not perfectly accurate near $\Delta = \Delta_{\pi/2}$ where the in/out-coupling of the CRIGF is vanishing. Aside from this central value, the parameters are evolving as expected. For the resonant wavelength λ_0 and the Q factor, the evolution is almost identical to that estimated from the SHG as is evidenced by the quasi-superposition of the blue dots (resulting from the SHG signal fits) and the red dots (from the linear spectra fits) in Figs. 8 (a) and (b). The fraction γ of the incident beam that actually interacts with the GC is seen to be independent of the asymmetry offset Δ . Indeed, as we tested the various CRIGFs on the sample, the experimental conditions (polarization state and modal shape of the incident beam) were constant and a careful alignment procedure was applied to ensure minimal variations of the spatial overlap. Similarly, the balance between the forward radiation and total radiation from the localized mode, represented by α , does not change with the asymmetry Δ . This is expected as this ratio only depends on the vertical stack (and more precisely on the phase and the amplitude of the non resonant reflection). Lastly, as expected, the probability for the localized mode to be radiated out of the CRIGF by the GC, η_r , is decreasing for asymmetry offsets Δ nearing $\Delta_{\pi/2}$ where the GC coupling strength is null.

6. Physical discussion

We define Q_a and Q_r as the absorption-limited and radiative-coupling-limited Q -factors :

$$Q_{a,r} = \frac{Q}{\eta_{a,r}}. \quad (9)$$

Both these quantities, together with the SHG efficiency S_0 and the total Q factor as a function of the offset Δ , are plotted in Fig. 9.

In this figure, we observe critical coupling in CRIGFs. Indeed, when $Q_a = Q_r$, the internal intrinsic losses of the CRIGF are equal to the coupling losses by the GC, which corresponds to critical coupling. This is achieved for two offset values, $\Delta \simeq 130$ nm and $\Delta \simeq 295$ nm (vertical dashed lines), one on each side of $\Delta_{\pi/2}$ where the coupling is null. We observe that the efficiency of conversion S_0 is indeed maximum near the critical coupling, which is coherent with a maximum of excitation of the localized mode. We also see that Q_a is nearly constant with values $\simeq 6000$. These observations are in good agreement with the theoretical predictions of [12] for critical coupling in CRIGF.

From the estimated values of Q , η_r and λ_0 we can estimate the intrinsic losses k_a and coupling losses k_r for the localized mode expressed per unit length, using the relations :

$$k_r = \frac{\pi}{\lambda_0 Q_r} = \eta_r \frac{\pi}{\lambda_0 Q} \quad (10)$$

$$k_a = \frac{\pi}{\lambda_0 Q_a} = \eta_a \frac{\pi}{\lambda_0 Q} \quad (11)$$

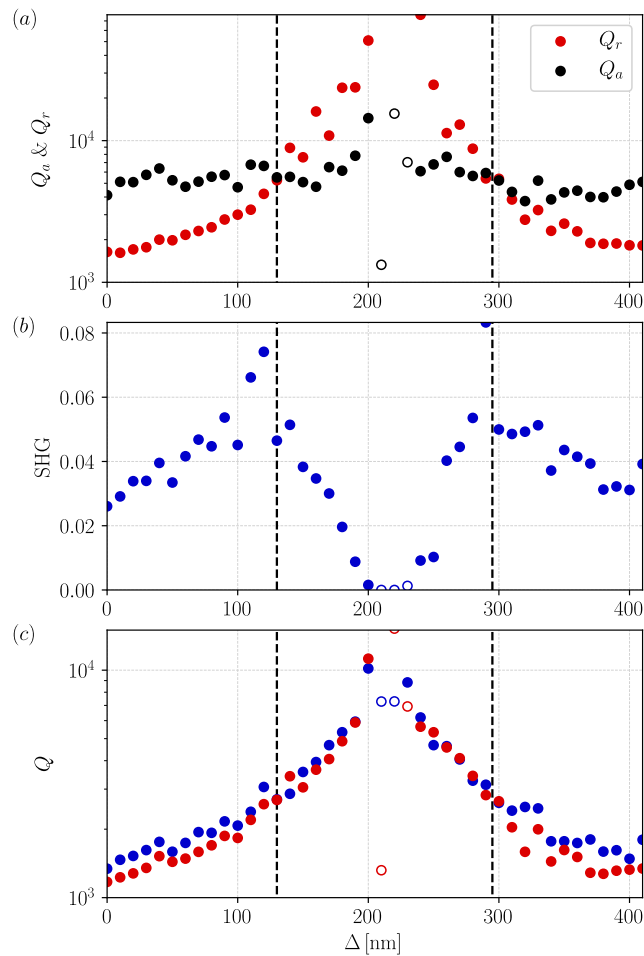


Fig. 9. Evolution with the asymmetry offset Δ of (a) the Q-factors associated to absorption Q_a (black dots) and to radiation coupling Q_r (red dots); (b) the SHG conversion efficiency (blue dots); (c) the Q factor of the corresponding CRIGFs as estimated from the SHG spectra (blue) and linear reflection and transmission spectra (red dots). Open dots correspond to unreliable fit results.

Figure 10 shows the obtained values as a function of Δ . As seen, the intrinsic losses (k_a , black dots) are almost constant, whilst the outcoupling losses (k_r , red dots) evolves as a $k_{r0} \cos^2(2\pi\Delta/\Lambda_{GC})$, with k_{r0} the maximal coupling losses obtained for a symmetric CRIGF ($\Delta = 0$). This evolution corresponds to the expected change with Δ in the overlap between the localized mode and the GC. Fitting of the constant value for k_a gives a value of $k_{a0} = 3.9 \pm 0.2$ [1/cm] (black line), while fitting of the amplitude k_{r0} gives $k_{r0} = 12.3 \pm 0.4$ [1/cm] (red line).

This further demonstrates that the asymmetric design of the GC allows to precisely control and adjust the coupling coefficient k_r of the GC and thus of the Q factor of the device, while keeping its intrinsic losses k_a unaffected.

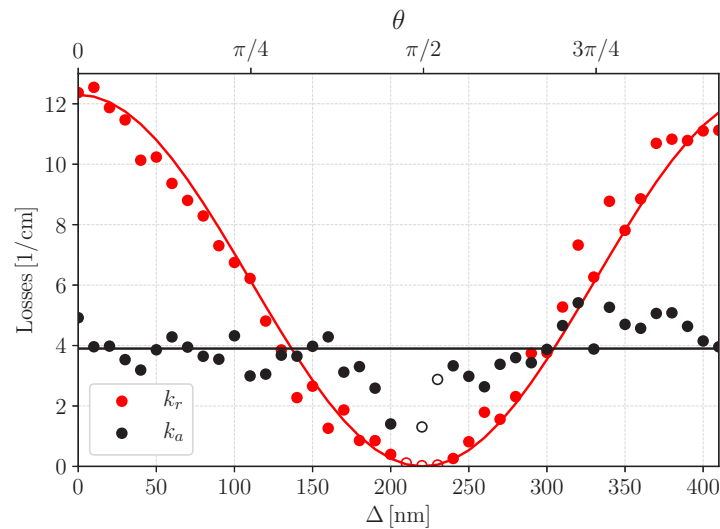


Fig. 10. Outcoupling losses k_r (red dots) and intrinsic losses k_a (black dots) as a function of the asymmetry offset Δ . The lines correspond to the expected evolutions rules, where the only fitting parameter are the amplitude of the squared cosine (red) and the constant value (black). (Open dots corresponds to offsets Δ for which the estimated values for k_r and k_a are not accurate.)

7. Conclusion

In conclusion, this study experimentally demonstrates several theoretical predictions. First, we evidence that the asymmetric GC design allows to easily control and tune the Q factor of a CRIGF from the over- to under-coupled regimes or vice-versa. Indeed, we can go from maximum to null coupling with a simple shift of the central coupler by 220 nm which has been readily implemented using e-beam lithography.

Second, we show that going from over- to under-coupled CRIGFs, the resonant reflectivity and transmission spectral signatures of the coupling reduce, and the SHG is maximised for critically-coupled resonators, confirming both predictions reported in [12].

Last, we introduced a new model that allows to estimate the physical parameters for CRIGFs, such as internal losses, which could not be done accurately with the previously available models. We have also proved that the results extracted from the linear and non-linear responses are self-consistent with, in particular, the detection and the agreement in the grating coupler position leading to the critical coupling condition.

The inferred intrinsic loss values are higher ($k_{a0} = 3.9 \pm 0.2$ [1/cm]) than what is typically achieved on the same material [25], suggesting that extra-losses are present in our devices. Finding the exact origin of these losses and methods to circumvent them are beyond the scope of this paper and will be the object of further work to fabricate CRIGFs whose experimental quality factors match the (ultra-high) values that have been theoretically predicted [12].

Funding. Agence Nationale de la Recherche.

Acknowledgements. This work was supported by French Defense Innovation Agency (AID) under grant ASTRID RESON ANR-19-ASTR-0019. The fabrication process realized in this work was done within the LAAS-CNRS cleanroom facilities, member of the national *RENATECH* platform network.

Disclosures. The authors declare no conflicts of interest.

Data availability. Data underlying the results presented in this paper are not publicly available at this time but may be obtained from the authors upon reasonable request.

References

1. C. W. Hsu, B. Zhen, A. D. Stone, J. D. Joannopoulos, and M. Soljačić, “Bound states in the continuum,” *Nat. Rev. Mater.* **1**(9), 16048 (2016).
2. S. I. Azzam and A. V. Kildishev, “Photonic Bound States in the Continuum: From Basics to Applications,” *Adv. Opt. Mater.* **9**(1), 2001469 (2021).
3. S. Joseph, S. Pandey, S. Sarkar, and J. Joseph, “Bound states in the continuum in resonant nanostructures: an overview of engineered materials for tailored applications,” *Nanophotonics* **10**(17), 4175–4207 (2021).
4. K. Kintaka, Y. Kita, K. Shimizu, H. Matsuoka, S. Ura, and J. Nishii, “Cavity-resonator-integrated grating input/output coupler for high-efficiency vertical coupling with a small aperture,” *Opt. Lett.* **35**(12), 1989–1991 (2010).
5. S. Augé, A. Monmayrant, S. Pelloquin, J. B. Doucet, and O. Gauthier-Lafaye, “Tunable graded cavity resonator integrated grating filters,” *Opt. Express* **25**(11), 12415 (2017).
6. S. Calvez, A. Monmayrant, and O. Gauthier-Lafaye, “Thermally-tunable cavity resonator-integrated guided-mode resonance filters,” *OSA Continuum* **2**(11), 3204 (2019).
7. A. Monmayrant, S. Calvez, P.-F. Calmon, P. Dubreuil, S. Charlot, A.-L. Fehrembach, E. Popov, and O. Gauthier-Lafaye, “Cavity resonator-integrated guided-mode resonance filters with on-chip electro- and thermo-optic tuning,” *Opt. Express* **30**(10), 16669–16676 (2022).
8. X. Buet, A. Guelmami, A. Monmayrant, S. Calvez, C. Tourte, F. Lozes-Dupuy, and O. Gauthier-Lafaye, “Wavelength-stabilised external-cavity laser diode using cavity resonator integrated guided mode filter,” *Electron. Lett.* **48**(25), 1619–1621 (2012).
9. S. Augé, S. Gluchko, A. L. Fehrembach, E. Popov, T. Antoni, S. Pelloquin, A. Arnoult, G. Maisons, A. Monmayrant, and O. Gauthier-Lafaye, “Extended cavity quantum cascade laser with cavity resonator integrated grating filter,” *Opt. Express* **28**(4), 4801 (2020).
10. C. Karnutsch, C. Pflumm, G. Heliotis, J. C. deMello, D. D. C. Bradley, J. Wang, T. Weimann, V. Haug, C. Gärtner, and U. Lemmer, “Improved organic semiconductor lasers based on a mixed-order distributed feedback resonator design,” *Appl. Phys. Lett.* **90**(13), 131104 (2007).
11. F. Renaud, A. Monmayrant, S. Calvez, O. Gauthier-Lafaye, A.-L. Fehrembach, and E. Popov, “Second-harmonic-generation enhancement in cavity resonator integrated grating filters,” *Opt. Lett.* **44**(21), 5198 (2019).
12. E. Popov, E. Hemsley, A.-L. Fehrembach, O. Gauthier-Lafaye, A. Monmayrant, and S. Calvez, “Extreme enhancement of the quality (Q)-factor and mode field intensity in cavity-resonator gratings,” *Opt. Express* **30**(14), 25390 (2022).
13. J. R. Piper and S. Fan, “Total absorption in a graphene monolayer in the optical regime by critical coupling with a photonic crystal guided resonance,” *ACS Photonics* **1**(4), 347–353 (2014).
14. S. Xiao, T. Liu, X. Wang, X. Liu, and C. Zhou, “Tailoring the absorption bandwidth of graphene at critical coupling,” *Phys. Rev. B* **102**(8), 085410 (2020).
15. K. Kintaka, K. Asai, K. Yamada, J. Inoue, and S. Ura, “Grating-Position-Shifted Cavity-Resonator-Integrated Guided-Mode Resonance Filter,” *IEEE Photonics Technol. Lett.* **29**(2), 201–204 (2017).
16. A.-L. Fehrembach, F. Renaud, E. Popov, H. Tortel, A. Monmayrant, O. Gauthier-Lafaye, and S. Calvez, “Dark mode-in-the-box for enhanced second-harmonic generation in corrugated waveguides,” *Opt. Express* **29**(25), 40981 (2021).
17. S. Fan, W. Suh, and J. D. Joannopoulos, “Temporal coupled-mode theory for the fano resonance in optical resonators,” *J. Opt. Soc. Am. A* **20**(3), 569–572 (2003).
18. J. W. Yoon and R. Magnusson, “Fano resonance formula for lossy two-port systems,” *Opt. Express* **21**(15), 17751 (2013).
19. D. Ding, M. J. A. de Dood, J. F. Bauters, M. J. R. Heck, J. E. Bowers, and D. Bouwmeester, “Fano resonances in a multimode waveguide coupled to a high-q silicon nitride ring resonator,” *Opt. Express* **22**(6), 6778–6790 (2014).
20. J. D. Joannopoulos, S. G. Johnson, J. N. Winn, and R. D. Meade, *Photonic Crystals: Molding the Flow of Light (Second Edition)* (Princeton University, 2008).
21. R. Laberdesque, O. Gauthier-Lafaye, H. Camon, A. Monmayrant, M. Petit, O. Demichel, and B. Cluzel, “High-order modes in cavity-resonator-integrated guided-mode resonance filters (CRIGFs),” *J. Opt. Soc. Am. A* **32**(11), 1973–1981 (2015).
22. X. Buet, E. Daran, D. Belharet, F. Lozes-Dupuy, A. Monmayrant, and O. Gauthier-Lafaye, “High angular tolerance and reflectivity with narrow bandwidth cavity-resonator-integrated guided-mode resonance filter,” *Opt. Express* **20**(8), 9322–9327 (2012).
23. A. Watanabe, K. Ozawa, R. Ueda, J. Inoue, K. Kintaka, and S. Ura, “An apodization method for guided-mode resonance grating with waveguide cavity,” *Jpn. J. Appl. Phys.* **61**(SK), SK1008 (2022).
24. B. Everitt and D. C. Howell, *Encyclopedia of statistics in behavioral science* (John Wiley & Sons, 2005).
25. I. Krasnokutskaya, J.-L. J. Tambasco, X. Li, and A. Peruzzo, “Ultra-low loss photonic circuits in lithium niobate on insulator,” *Opt. Express* **26**(2), 897 (2018).